IMPEDANCES FOR ELECTRON LINACS AND STORAGE RINGS

Perry B. Wilson

Stanford Linear Accelerator Center

In this note some basic concepts and results are presented concerning the impedances of electron linacs and storage rings. The impedance of an accelerator or ring completely characterizes the interaction of the beam with its environment. Not only does the impedance (or its Fourier transform, the wake potential) determine the energy loss by a bunched beam to its environment, but it is also the chief ingredient required for any calculation of beam stability.

As the title implies, we will be concerned mainly with particles moving close to the velocity of light. The assumption $v \approx c$ makes possible certain important simplifications in the impedance-wake potential formalism but, unfortunately, it is clearly violated in the case of heavy ion accelerators. In several instances we will point out where it might be possible to extend the results to the more general case.

Another limitation in the present note is that it is concerned almost entirely with the longitudinal impedance. A parallel development is often possible for the case of the transverse impedance, but the analysis, measurement methods and computer programs tend to be more complicated. At SLAC, the effort being directed to the measurement and computation of transverse impedances is just now reaching the level that was earlier devoted to the longitudinal impedance problem. For example, a computer program is just being completed for calculating the transverse deflection modes in the SLAC linac structure.

Some Definitions

A loss parameter $k(\sigma)$, defined by

$$k(\sigma) = \frac{\Delta U}{q^2}$$

gives the total energy loss ΔU given up to a component by a bunch with charge q and bunch length σ. For a periodic train of bunches spaced in time by T_b, the loss parameter determines the average power loss to a component by

$$P = I_o^2 k T_b = I_o^2 Z_\ell \tag{1}$$

where $Z_\ell = kT_b$ is the loss impedance and I_o the average current. The impedance function for a component is defined by (see Fig. 1),

$$Z(\omega) = \frac{V(\omega)}{I(\omega)} .$$

The wake function, or wake potential $w(\tau)$, is the potential seen by a non-perturbing test charge following at time τ behind a unit charge passing through a component. The net potential at time t in a charge distribution I(t) is then obtained as

$$V(t) = \int_{-\infty}^{t} w(t-\tau) I(\tau) d\tau. \tag{2}$$

The following transform relations between the frequency and time domain can be shown to hold (a tilda indicates the Fourier transform):

$$I(\omega) = \tilde{I}(t)$$

$$V(\omega) = \tilde{V}(t)$$

$$Z(\omega) = \pi\tilde{w}(t).$$

Some Consequences

The impedance function $Z(\omega)$ is in general a complex function,

$$Z(\omega) = Z_R(\omega) + jZ_I(\omega).$$

If we take $w(\tau)$ to be a real function of time, then it follows that

$$Z_R(\omega) = Z_R(-\omega) \qquad \text{(an even function of } \omega)$$
$$Z_I(\omega) = -Z_I(-\omega) \qquad \text{(an odd function of } \omega).$$

If the velocity of a particle passing through a component is close to the velocity of light, then the wake potential is causal, or nearly so. That is, $w(\tau) \equiv 0$ for $\tau < 0$. Then we can show that $Z_R(\omega)$ and $Z_I(\omega)$ are related by the Hilbert transform,

$$Z_I(\omega) = \frac{1}{\pi} \int_{-\infty}^{\infty} \frac{Z_R(\omega')}{\omega' - \omega} \, d\omega'. \tag{3}$$

Thus a knowledge of $Z_R(\omega)$ is sufficient to determine $Z_I(\omega)$. However, the wake induced in a component by a charge will not vanish ahead of the charge. The assumption of a causal wake potential also implies that

$$w(\tau) = \frac{2}{\pi} \int_0^{\infty} Z_R(\omega) \cos\omega\tau \, d\omega. \tag{4}$$

Under the assumption that $I(t)$ is a real function of time, the loss parameter $k(\sigma)$ can also be related to the real part of the impedance function by

$$k(\tau) = \frac{\pi}{q^2} \int_0^{\infty} I^2(\omega) \, Z_R(\omega) \, d\omega \, .$$

For a Gaussian bunch this reduces to

$$k(\tau) = \frac{1}{\pi} \int_0^\infty Z_R(\omega) e^{-\omega^2 \sigma_t^2} \, d\omega. \tag{5}$$

Application to Resonant Modes

For a high-Q parallel resonant circuit, we have

$$Z(\omega) = \frac{R}{1+j2Q\delta}$$

$$Z_R(\omega) = \frac{R}{1+(2Q\delta)^2}$$

where $\delta = (\omega - \omega_0)/\omega_0$. From this relation and Eq. (4) in the preceding section we derive for the n^{th} mode,

$$w(\tau) = 2k_n \cos \omega_n \tau$$

$$k_n = \frac{\omega_n}{4} \left(\frac{R}{Q}\right)_n = \frac{V_n^2}{4W_n}$$

where V_n is voltage gain for a non-perturbing test charge when W_n is the stored energy. The total wake potential for a resonator is the sum over all modes,

$$\omega(\tau) = 2 \sum_n k_n \cos\omega_n\tau \quad . \tag{6}$$

The total loss parameter for a bunch with bunch length σ_t is

$$k(\sigma_t) = \sum_n k_n \, e^{-\omega_n^2 \sigma_t^2} \, . \tag{7}$$

Two computer programs exist for computing ω_n and k_n for the fundamental and higher-order longitudinal modes in cavities and structures. The program KN7C[1] computes modes for a periodic structure characterized

by the four parameters a, b, g and d shown in Fig. 2. A single resonant cell can be modeled by setting d - g >> a. Similarly, the program SUPERFISH[2] computes modes for a single axi-symmetric cavity having any boundary in the r-z plane. That is, the function r(z) representing the surface can be arbitrary, even multiply connected. However, any cross-section in the r-ϕ plane must be a circle. In addition to values for ω_n, k_n and Q_n, the E and H fields at any point in the cavity can also be obtained from the output. By putting a taper in the beam tube as shown at the right in Fig. 1, the loss to small discontinuities such as a gap or iris can be obtained from SUPERFISH, even though there are no standing-wave modes in the gap or iris region.

An example of the power of SUPERFISH is its application to the computation[3] of modes in the RF cavities for PEP and the proposed LEP storage ring (which uses PETRA-type cavities scaled to 353 MHz). Fig. 3 shows the cavity dimensions, and Fig. 4 gives sketches of the electric field patterns for the first 9 higher-order modes in the PETRA-type cavity. Table I gives numerical values for the properties of the 19 standing-wave modes below cutoff of the beam tube. These results define, in fact, the impedance function for this RF cavity. For large rings such as PEP or PETRA the impedance of the RF system is the major part of the total ring impedance. Thus for these rings there is little uncertainty as to the ring impedance, since the largest contribution can be computed with good accuracy. Finally, Fig. 5 shows how the loss parameter for loss to higher order modes (k_{hom}) and the total loss parameter (k_{tot}) for these cavities depend strongly on bunch length.

Table I

PETRA CAVITY MODES

Mode Number and Type				Frequency (MHz)	R/Q (ohms)	Q_o (x 10^{-3})		k (V/pc)
1	Even	11,00		359.2	250.4	47.2		0.1413
2	Odd	11,11		525.0	55.6	40.5		0.0458
3	Even	21,20		886.5	9.4	71.5		0.0130
4	Odd	22,11		974.0	44.2	26.1		0.0677
5	Even	22,22		1221.1	17.0	39.8		0.0327
6	Odd	21,31		1237.4	4.1	26.5		0.0080
7	Even	33,00		1396.0	7.7	99.5		0.0168
8	Odd	32,31		1466.1	2.3	24.6		0.0054
9	Odd	22,33		1564.8	5.5	20.9		0.0134
10	Even	21,42	(31,22)	1588.0	6.6	38.2	(68.5)	0.0165
11	Even	32,42		1700.6	4.6	71.4	(66.7)	0.0123
12	Even	33,40	(43,20)	1854.7	1.9	--	(59.9)	0.0054
13	Odd	43,31		1888.3	4.3	71.4	?	0.0129
14	Even	24,40		1931.5	0.2	108.5		0.0007
15	Odd	44,11		1990.3	6.6	23.4		0.0206
16	Odd	12,53		2035.5	1.4	18.1	(70.4)	0.0045
17	Even	43,42		2107.3	0.3	72.8		0.0011
18	Odd	32,31		2220.0	0.4	70.2		0.0016
19	Even	34,42	(44,22)	2261.2	6.2	78.2		0.0219
	Cutoff Frequency			(2295)				
20	Odd	43,53		2355.4				0.0030
21	Even			2372.3				0.0002
22	Even			2416.9				0.0005
23	Odd			2429.2				0.0012
24	Even			2492.2				0.0036
25	Even			2558.8				0.0001
26	Odd			2587.6				0.0002

A transverse version of KN7C has just been completed[4]. This code will calculate the deflection modes for the periodic structure shown in Fig. 2. The first use of the program will be to compute the transverse deflection mode for the SLAC two-mile linac in order to predict the emittance growth for single bunches. This computation is important for predicting the luminosity that can be achieved by the proposed linac collider project.

Measurement Techniques

Figure 6 shows the measurement method, originally proposed by Sands and Rees[5], that has been used to measure the loss parameter $k(\sigma)$ for the PEP ring components. Elaborations of this method were also used at PETRA and CESR[6]. In this method, an approximately Gaussian pulse is sent along a wire on the axis of the component to be tested. The pulse will interact with any mode having (in the absence of the wire) an E_z field on the axis. The excited fields or modes will induce a secondary pulse, $I_s(t)$, on the wire. As shown in Fig. 7, the net pulse $I_1(t)$ observed at the output of the component is a superposition of $I_s(t)$ and the incident pulse $I_0(t)$: $I_1(t) = I_0(t) + I_s(t)$. The incident pulse is obtained by substituting a smooth reference pipe for the component. If the incident pulse could be made arbitrarily short (a delta-function), then for $t > 0$, $I_s(t) = I_1(t)$ would be proportional to the wake potential $w(t)$.

The total loss parameter is given[5] by

$$k = \frac{2Z_0}{q^2} \int I_0(t)\, I_s(t)\, dt$$

$$q = \int I_0(t)\, dt$$

where Z_0 is the characteristic impedance of the reference pipe with the wire in place. By using incident pulses of different length, the

loss can be measured as a function of bunch length. Using this measurement method, the loss parameter k has been measured for all PEP components at a bunch length of 2.3 cm. Detailed results are given in Ref. 7. Some representative results for gaps, tapers and chambers are shown in Fig. 8. By adding up the loss parameter for each component in PEP, a total loss parameter of $k \approx 35$ V/pC is obtained for the whole ring at $\sigma = 2.3$ cm. Of this total, 24 V/pC comes from higher modes in the RF cavities and about 11 V/pC from the remaining vacuum chamber components. Thus, the ring impedance is strongly dominated by the impedance of the RF cavities. For two 55 mA beams with $T_b = 2.45$ μs, the total power loss from Eq. (1) is 500 kW.

Measurements and theory have been compared[8] for several cylindrical cavities with beam tube holes. For example, $k(\sigma)$ was measured and computed for the cavity shown in Fig. 7 for bunch lengths of 110, 240 and 350 ps. Using Eq. (7) with output from either KN7C or SUPERFISH for ω_n and k_n (the two programs give consistent results), values of $k(\sigma) = 0.144$, 0.054 and 0.018 were computed for these bunch lengths. The measured values were $k(\sigma) = 0.146$, 0.055 and 0.018 with a resolution of about ±.003.

A more detailed comparison can be made between theory and measurement using the difference function $I_s(t)$. Within the pulse the measured potential for $I_s \ll I_o$ is

$$V(t) = 2Z_0 \ I_s(t) \ .$$

From Eq. (2) the computed potential for a Gaussian pulse with peak

amplitude Ip is

$$V(t) = Ip \int_0^\infty w(\tau)\, e^{-(t-\tau)^2/2\sigma_t^2}\, d\tau.$$

The wake potential is obtained using Eq. (6) and the output of KN7C or SUPERFISH. In Fig. 9 the measured and computed functions are compared, with no adjustable constants used in obtaining the theoretical curves. The agreement enhances confidence both in the theory and in the measurement technique.

Frequency domain measurements can also be made using the stretched wire technique with a frequency sweep generator in place of the pulse generator at the input taper in Fig. 6. The transmission through the component is monitored by a detector at the output taper. At the frequency of each resonant longitudinal mode, a dip in the transmitted power is seen. From the area under the dip, the R/Q for the mode can be computed. The Q of the mode is, of course, drastically lowered by the presence of the wire, but R/Q can still be obtained if the modes do not overlap. An equivalent statement for pulse measurements in the time domain is that effects depending on the short-range wake are measured correctly, but the time decrement for the long-range wake is too fast. By moving the wire off-axis, the R/Q's can be measured for deflection modes using the same technique. Reasonable agreement is obtained with analytic results in those cases where a comparison is possible.

In principle it is possible to make either time or frequency domain measurements for the case $v < c$ using the wire technique. The "wire" in this case must be a loaded line (e.g., helix wound on a thin dielectric rod) with a phase velocity equal to the desired particle velocity.

Again, only the R/Q's of resonant modes can be measured in the frequency domain, losses, corresponding to the short-range wake in the time domain.

Wake Potential for the SLAC Linac

The structure shown in Fig. 2a is a reasonable approximation to the disk-loaded structure of the two-mile SLAC linac. Using output from KN7C in Eq. (6) for 416 modes, the wake function for SLAC was computed[9]. The result is shown in Fig. 10. In addition to the wake computed from the modes, the result also includes the contribution of an "analytic extension", which takes into account the effect of modes beyond the highest frequency reached by the computer calculation. The analytic extension uses the Sessler-Vainshtein optical resonator model described in Ref. 1. It covers the frequency range from $\omega = 6.1 \times 10^{11}$ (for the 416th mode) to $\omega = 8 \times 10^{13}$. (The fundamental mode is at $\omega = 1.8 \times 10^{10}$.) The contribution of the analytic extension is important only for the first picosecond or so.

Using Eq. (7) the average energy loss per particle can be computed. The computed loss is 40 MeV per electron, while the measurements give 50 MeV. Considering the possible experimental errors in the measurement, this is reasonable agreement. The average energy loss is related to the intercept of the wake potential at t = 0. From Eqs. (6) and (7), $w(0) = 2k$ for a point bunch. The time dependence of the wake affects the detailed shape of the energy spectra. In Ref. 9 it is shown that detailed agreement between measured energy spectra and spectra computed from the wake in Fig. 10 is very good, if the amplitude of the computed wake is multiplied by a factor of 1.3.

The SPEAR Impedance Function

The impedance function for SPEAR is shown in Fig. 11. The form of this function was obtained as follows. From data[10] on bunch lengthening in SPEAR, it can be shown[11] that at high frequencies the real part of the impedance must vary as $Z_R(\omega) \sim \omega^{-0.68}$. However, at low frequencies the impedance must fall to zero. Quite arbitrarily the low frequency portion is represented by a linear dependence on frequency. Thus, $Z_R(\omega)$ has a maximum value Z_0 at some frequency $\omega_0 = 2\pi f_0$ where the two curves intersect. Using Eq. (5), Z_0 and f_0 can be adjusted to fit measured energy loss data for SPEAR. This loss is represented quite accurately for SPEAR by

$$k(\sigma) = \left[50\ \sigma_z(\text{cm})\right]^{-1.21}\ \text{V/pC}. \qquad (8)$$

The result of the fitting procedure (described in Ref. 12) is $Z_0 = 8000$ ohms and $f_0 = 1.2$ GHz.

The imaginary part of the impedance can be computed, if the real part is given, using the Hilbert transform in Eq. (3). The result[13] is shown in normalized form in Fig. 11. The ratio Z/n is also of interest in predicting the threshold for various beam instabilities, where n is the harmonic number of the revolution frequency (1.28 MHz for SPEAR). From Fig. 11 we readily compute $Z_R/n = 8.5$ ohms. The total impedance $|Z|/n$ is on the order of 20 ohms.

Comparison of SPEAR and PEP Impedances

Some impedances for SPEAR and PEP are compared in Table II below. Using Eq. (7) and the definition of the loss impedance, $Z_\ell = T_b k(\sigma)$,

the total SPEAR impedance at a bunch length of 2.0 cm is computed to be Z_ℓ = 17 MΩ. Computer calculations using SUPERFISH and KN7C give a loss impedance of 3 MΩ for higher-order modes in the RF cavities. This leaves 14 MΩ for the vacuum chamber loss. Thus, losses in the vacuum chamber external to the RF cavities are dominant for SPEAR. PEP has six times more RF cavities than SPEAR, but the beam hole size is somewhat smaller on the average and the loss per cavity is about 24% greater. Remember also that the loss impedance for a given component scales in proportion to the time between bunches: $T_b(\text{PEP})/T_b(\text{SPEAR}) = 3.13$. Applying these factors gives a loss impedance for the PEP cavities of 69 MΩ. The loss for the PEP vacuum chamber, on the other hand, has been measured to be about 8% of the loss per unit length for SPEAR. The total circumference of PEP is greater by a factor of 9.4. Multiplying the SPEAR vacuum chamber impedance by 3.13 x 9.4 x .08 gives 33 MΩ for PEP. We see that for PEP the cavity impedance is about twice the vacuum chamber impedance. Estimated values for Z_R/n and $|Z|/n$ are also given in Table II for SPEAR and PEP.

TABLE II

Impedances for SPEAR and PEP

at σ_z = 2.0 cm

		SPEAR	PEP
Z_ℓ(rf)	MΩ	3 (18%)	69 (68%)
Z_ℓ(vac)	MΩ	14 (82%)	33 (32%)
Z_ℓ(tot)	MΩ	17	102
Z_R/n	ohms	8.5	1.8
$\|Z\|/n$	ohms	≈ 20	≈ 4

Impedances, Wakes and Stability

Analytic stability criteria have been developed so far mainly in the frequency domain. A solution in the form of an expansion in modes is first obtained, with mode frequencies that may be complex. As some parameter (such as charge per bunch) is increased, the imaginary part of the frequency for a particular mode may change sign, indicating a transition from damping to exponential growth. However, in order to carry the procedure past the stage of a very general expression, simplifying assumptions are usually introduced which limit the predictive power of the model.

In the time domain, non-linear problems are usually attacked by computer simulations using a limited number of superparticles. The coupling between particles is characterized by the wake potential, rather than the impedance. It is difficult, however, to develop analytic criteria for stability. A recipe for obtaining stability criteria similar to that outlined above for the frequency domain, does not appear to exist. The situation may be changing with the recent interdisciplinary surge of interest in non-linear dynamics[14]. For the case of turbulent bunch lengthening an unusual time-domain stability criteria has been developed[15], which may have an application to other aspects of the problem of the interaction of a charged beam with its environment.

References

1. E. Keil, Nucl. Instr. Methods 100, 419 (1972).

2. K. Halbach and R.F. Holsinger, Part. Accel. 7, 213 (1976).

3. P.B. Wilson, LEP-70/69, CERN (May 1978).

4. B. Zotter and K. Bane, PEP Note-308, SLAC (1979).

5. M. Sands and J. Rees, PEP-95, SLAC (1974).

6. M.G. Billing, J.L. Kirchgessner and R.M. Sundelin, IEEE Trans. Nucl. Sci. NS-26, 3583 (1979).

7. J.N. Weaver, P.B. Wilson and J.B. Styles, IEEE Trans. Nucl. Sci. NS-26, 3971 (1979).

8. P.B. Wilson, J.B. Styles and K.L.F. Bane, IEEE Trans. Nucl. Sci. NS-24, 1496 (1977).

9. R.F. Koontz, G.A. Loew, R.H. Miller and P.B. Wilson, IEEE Trans. Nucl. Sci. NS-24, 1943 (1977).

10. P.B. Wilson et al, IEEE Trans. Nucl. Sci. NS-24, 1211 (1977).

11. A.W. Chao and J. Gareyte, SPEAR-197/PEP-224, SLAC (1976).

12. P.B. Wilson, PEP-233, SLAC (1977).

13. K. Bane and P. Wilson, PEP-261, SLAC (1977).

14. Siebe Jorna, ed. Topics in Nonlinear Dynamics, AIP Conf. Proc. No. 46 (American Inst. of Physics, NY, 1978).

15. P.B. Wilson, PEP-232, SLAC (1977).

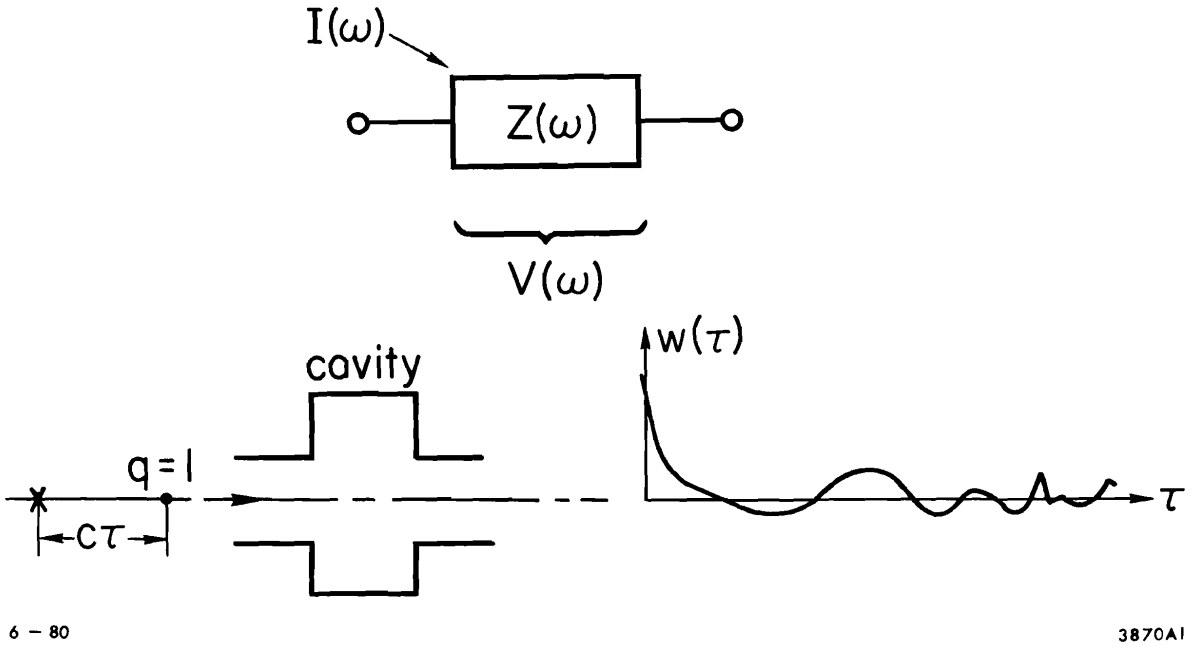

Fig. 1 -- Physical meaning of the impedance functions $Z(\omega)$ and wake potential $w(\tau)$.

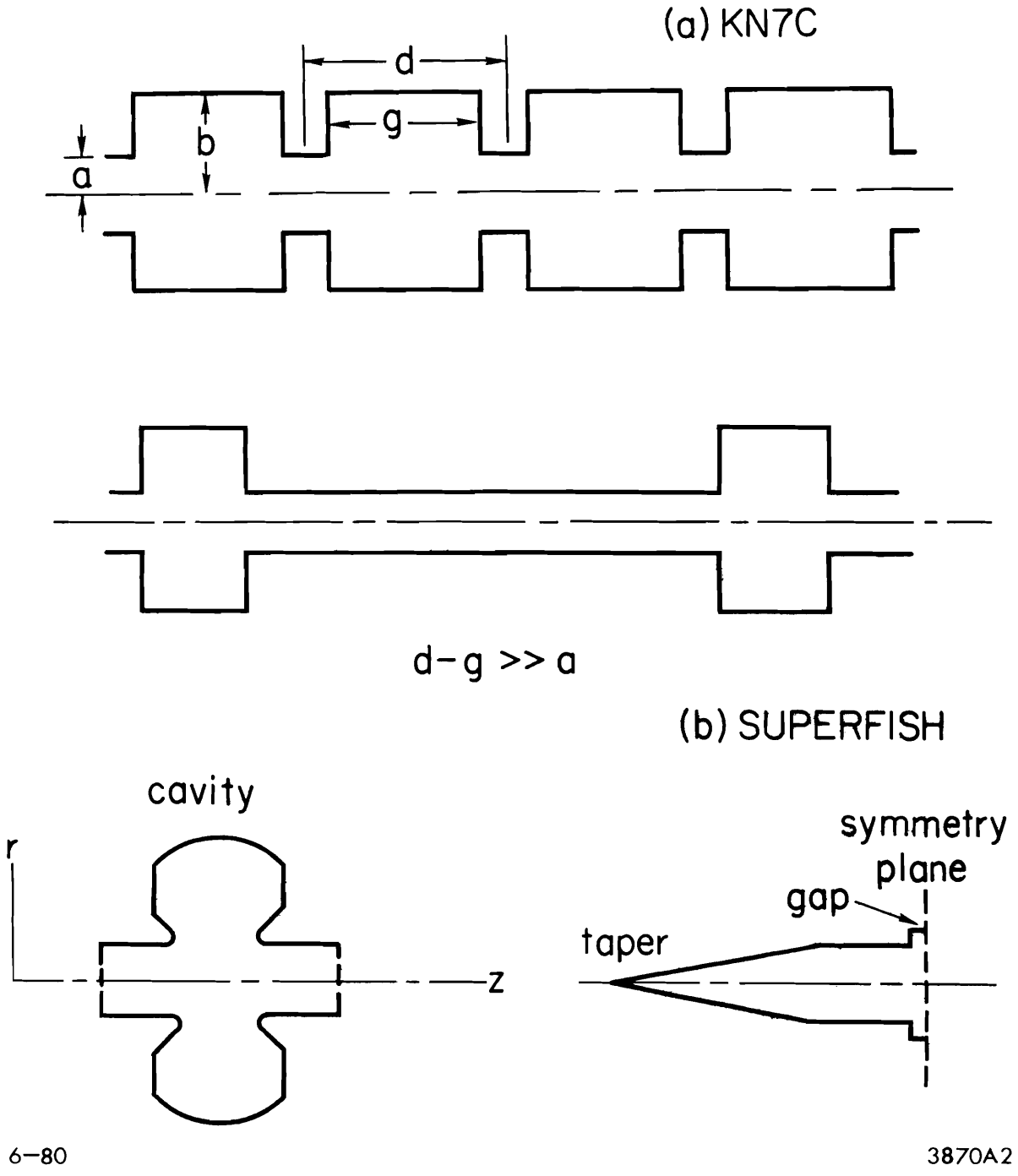

Fig. 2 -- Structures that can be computed by KN7C and SUPERFISH.

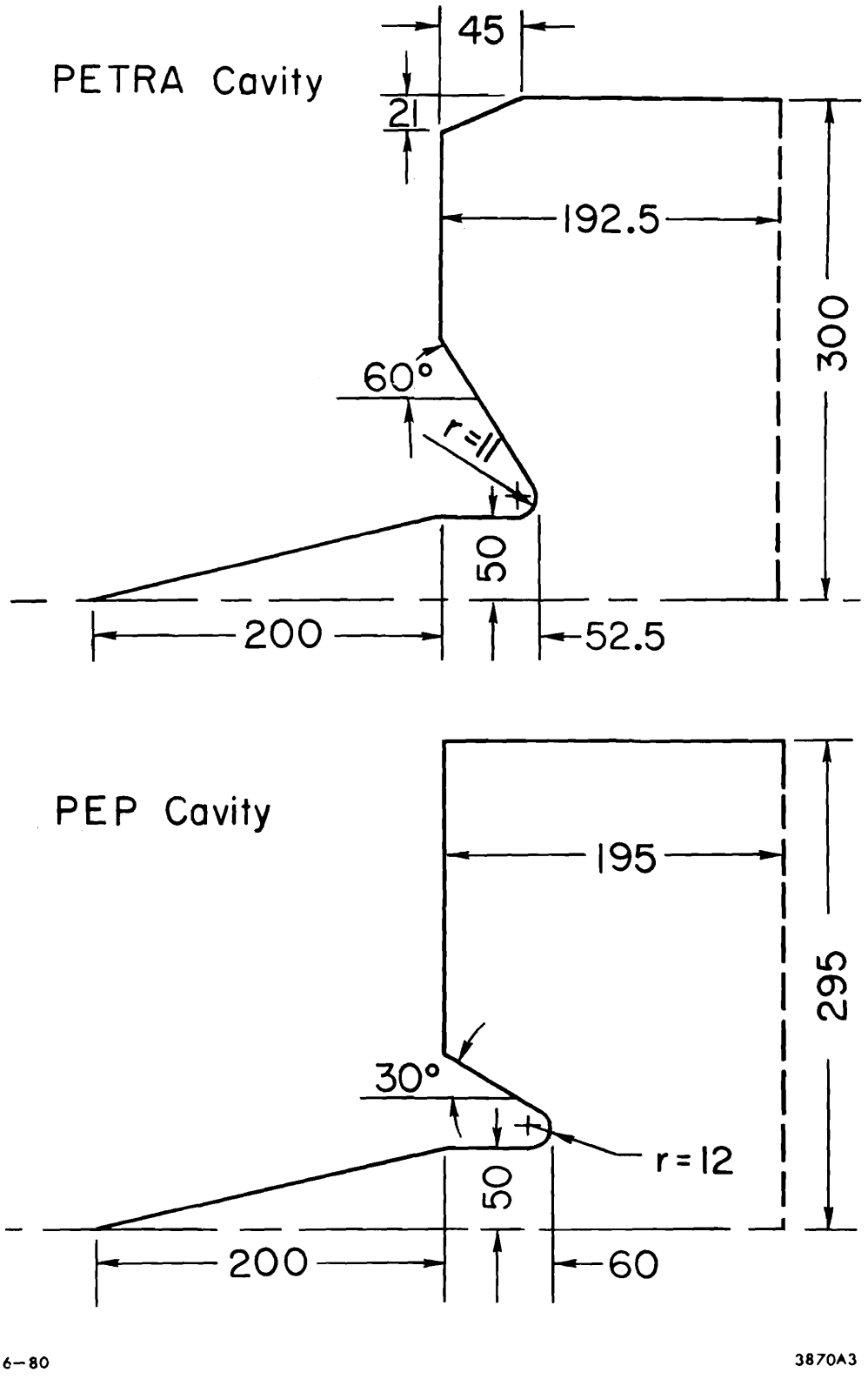

Fig. 3 -- Dimension of the PEP and PETRA cavities.

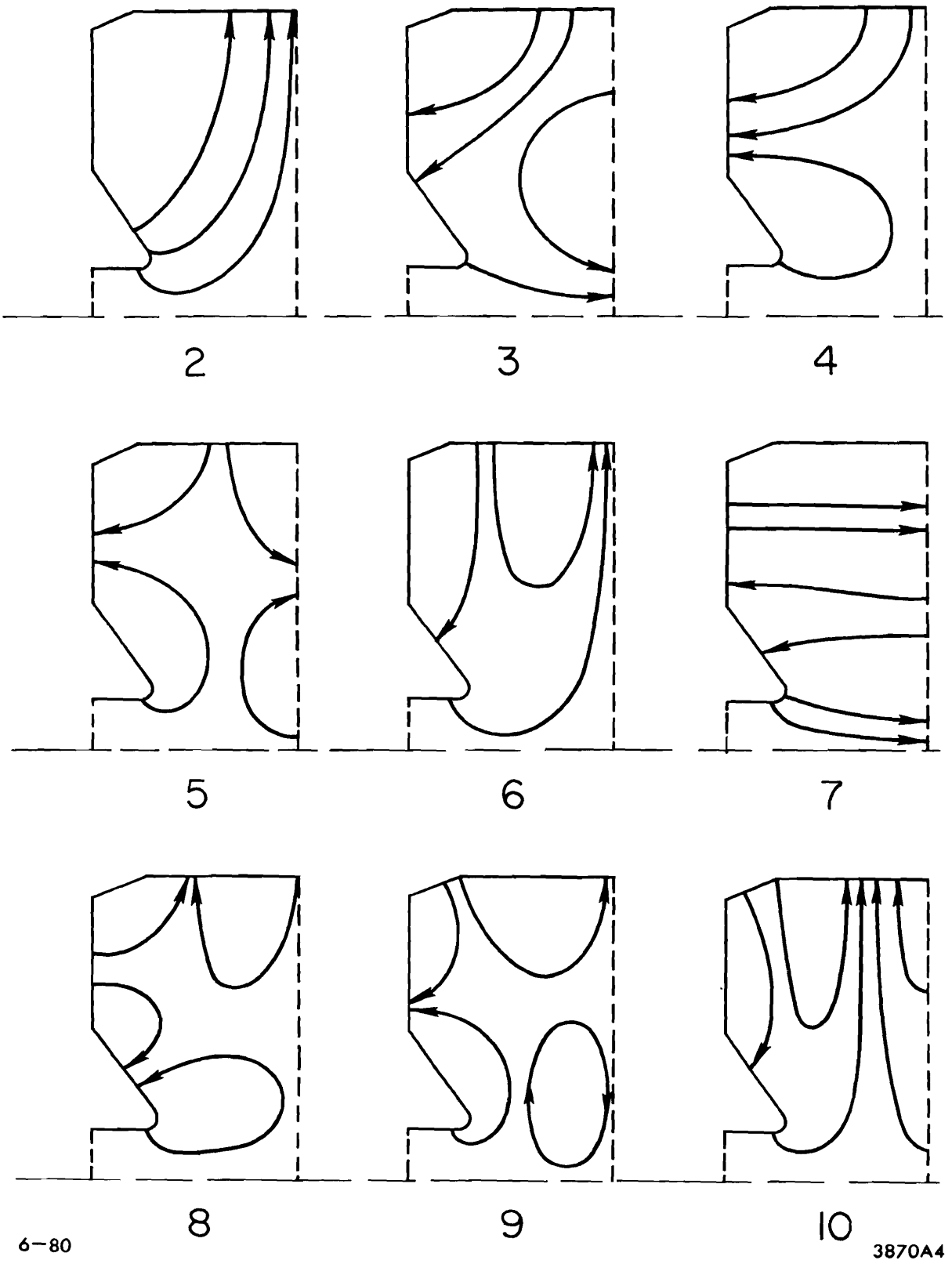

Fig. 4 -- Electric field for the first 9 higher-order modes in the PETRA-type cavity.

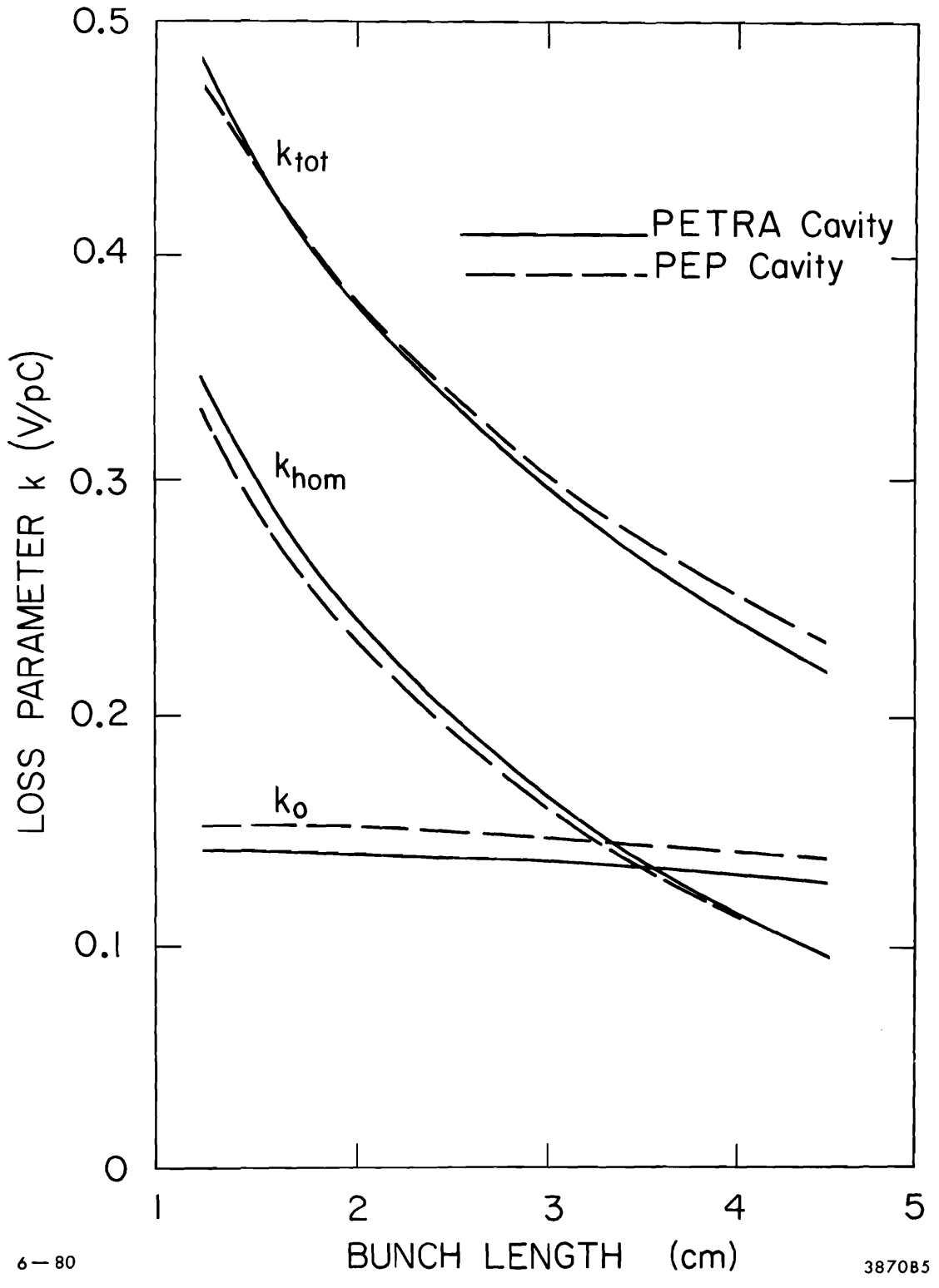

Fig. 5 -- Loss parameter as a function of bunch length for the PEP and PETRA cavities.

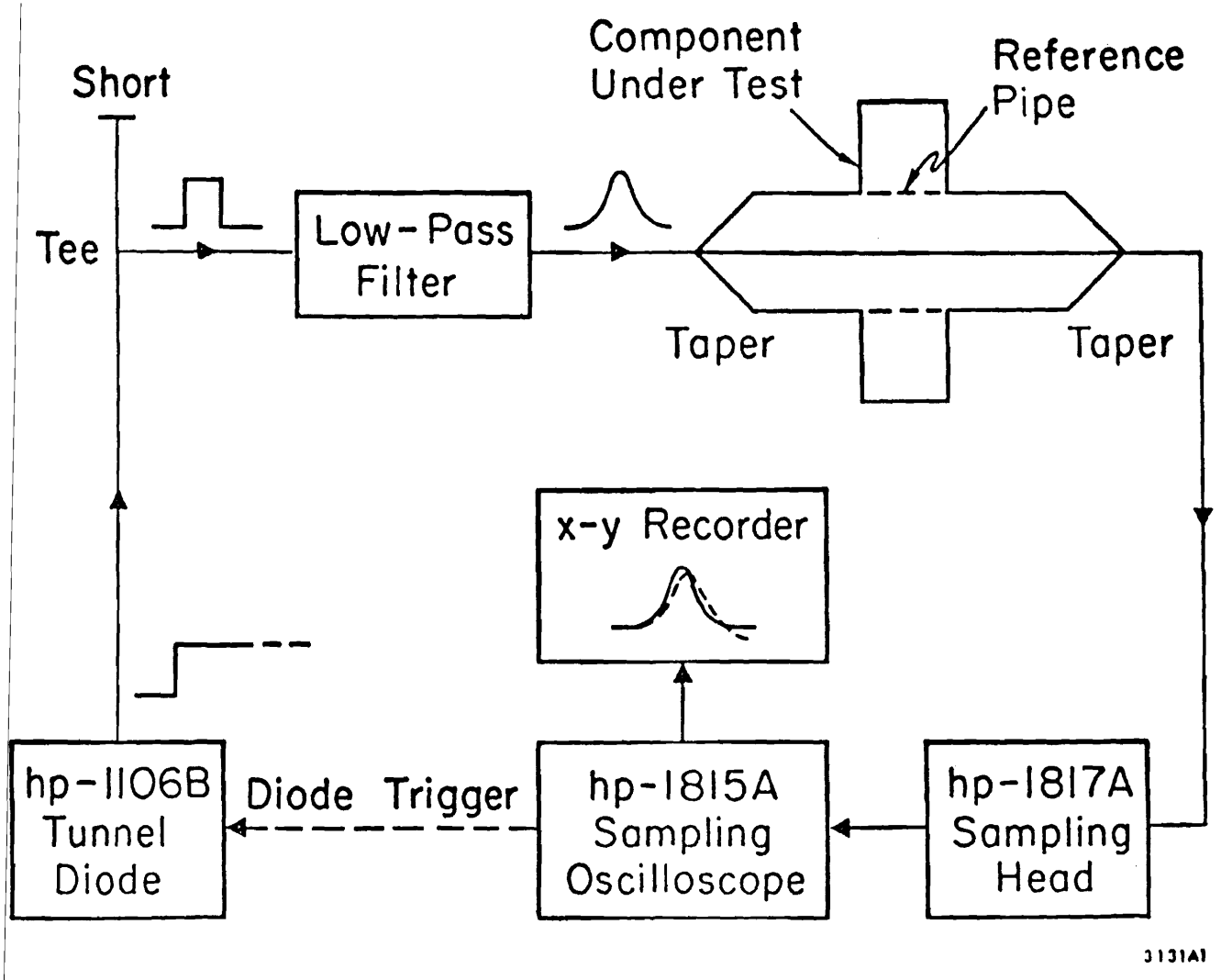

Fig. 6 -- Instrumentation for measuring the loss parameter.

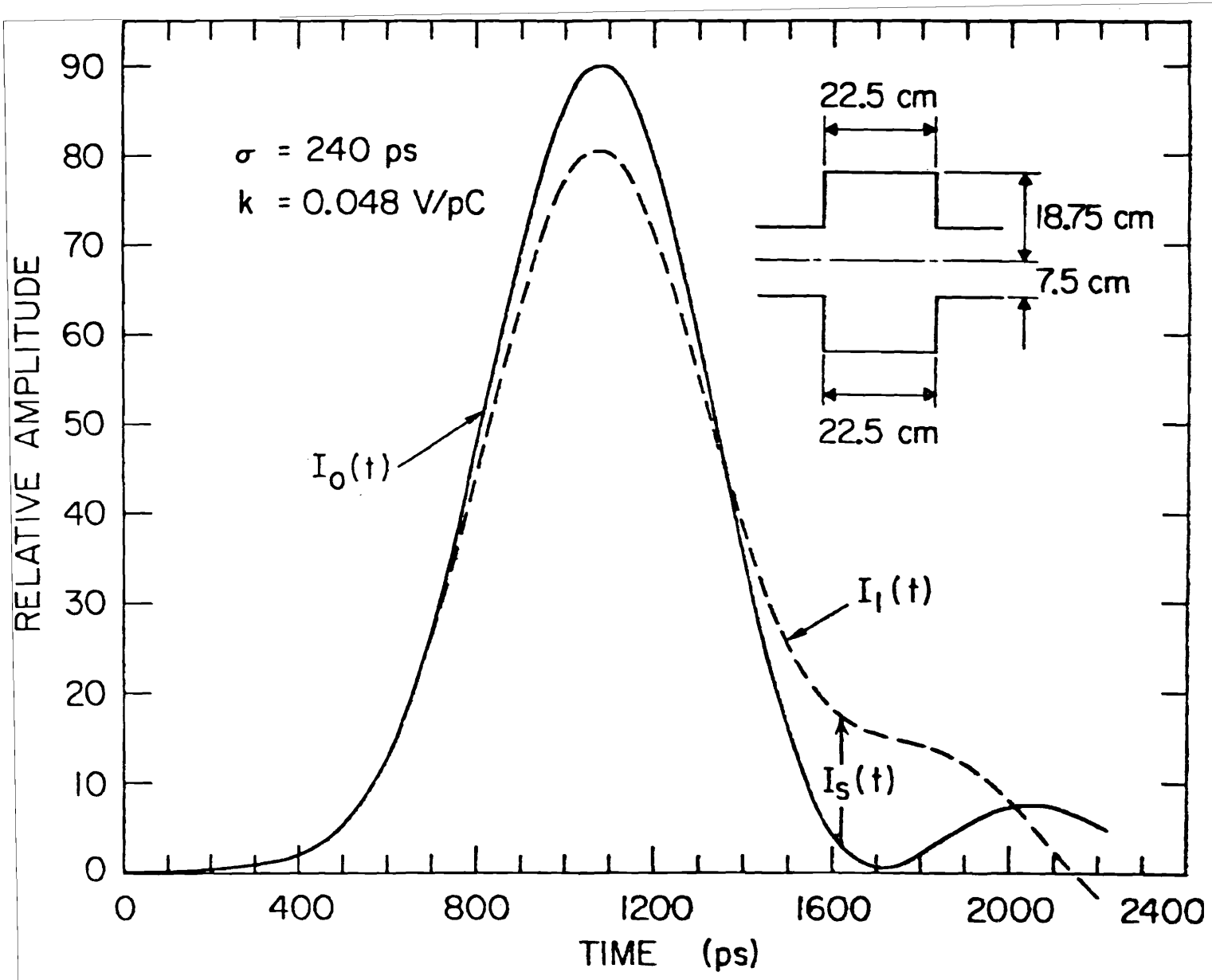

Fig. 7 -- Recorded output pulses $I_0(t)$ for the reference pipe and $I_1(t)$ for a cylindrical cavity having the dimensions shown.

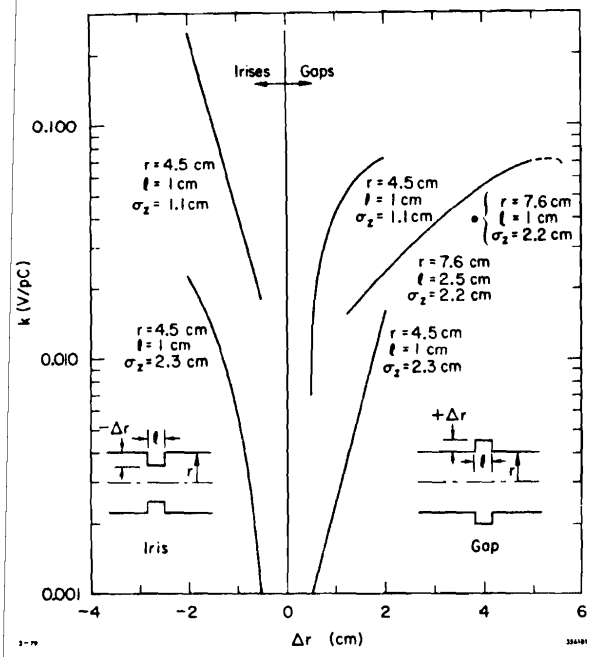

Radial gaps and irises.

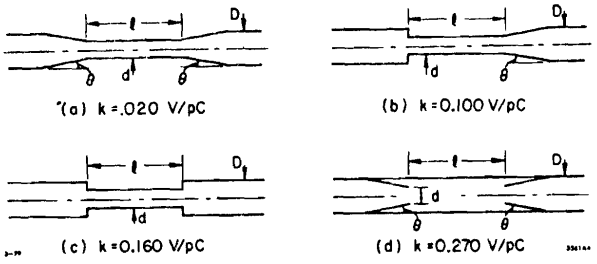

Collimator chambers. D_o = 20 cm diam, d = 10 cm diam, $\theta = 10^o$, ℓ = 56 cm and σ_z = 2.5 cm.

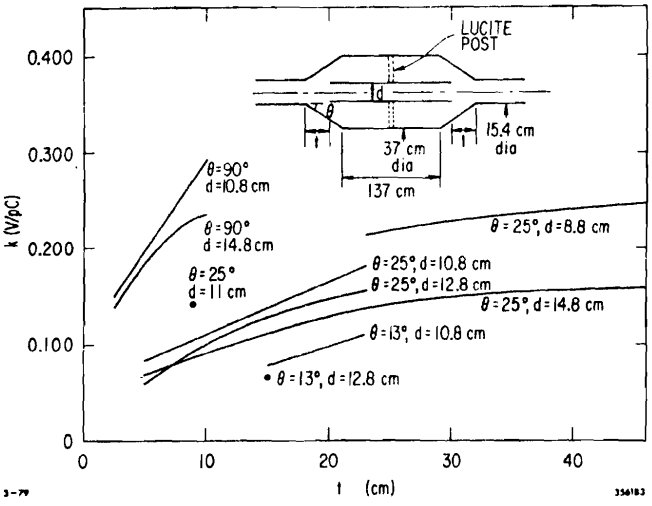

Separating plates model (σ_z = 2.3 cm).

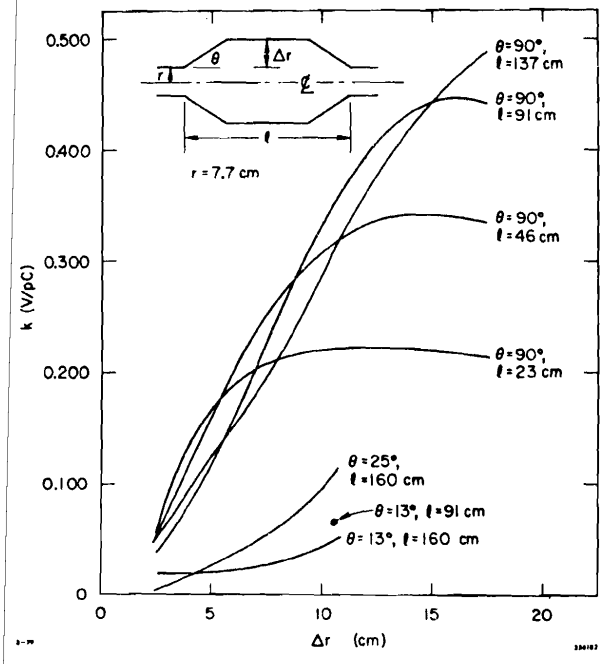

Tapers with various angles and spacings between tapers (σ_z = 2.3 cm).

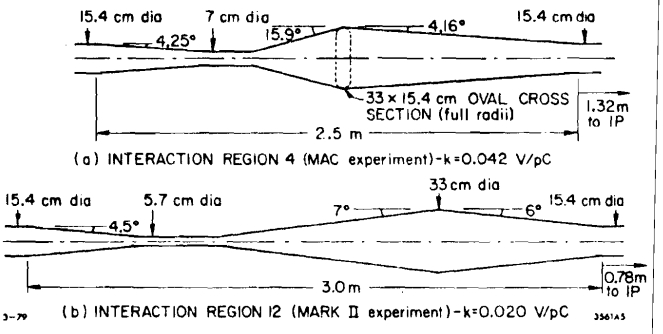

Interaction region chambers (σ_z = 2.3 cm). There is symmetry about the interaction point (IP), so the total loss is twice that given above.

Fig. 8 -- Loss parameters for some representative PEP components.

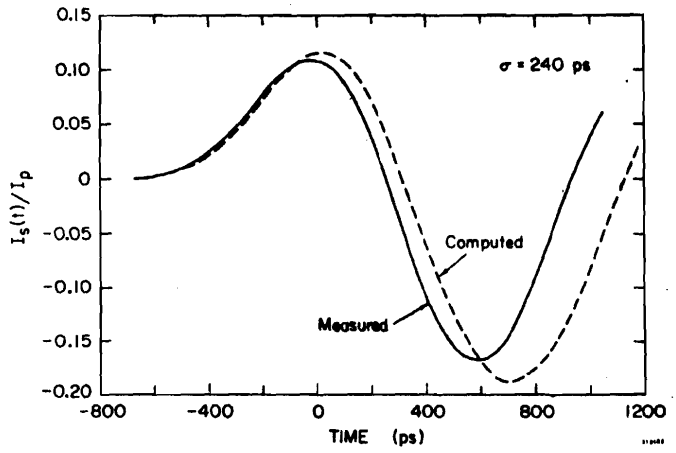

Fig. 9a Computed and measured functions $I_s(t)/I_p$ for the cavity shown in Fig. 7 for a bunch length $\sigma = 240$ ps.

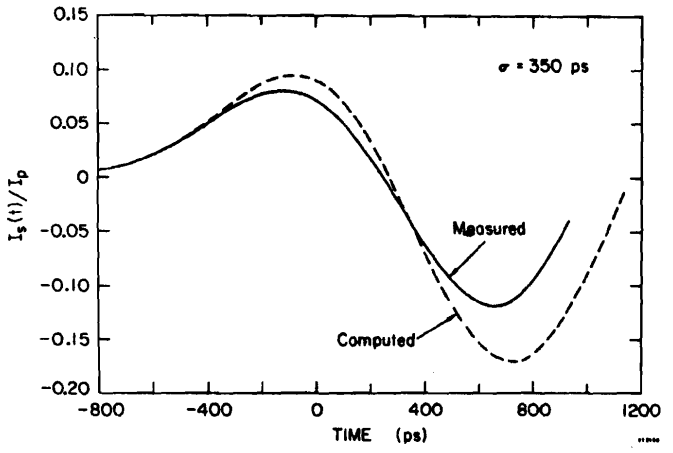

Fig. 9b Computed and measured functions $I_s(t)/I_p$ for the cavity shown in Fig. 7 for a bunch length $\sigma = 350$ ps.

Fig. 9 -- Computed and measured functions $I_S(t)/Ip$ for the cavity shown in Fig. 7.

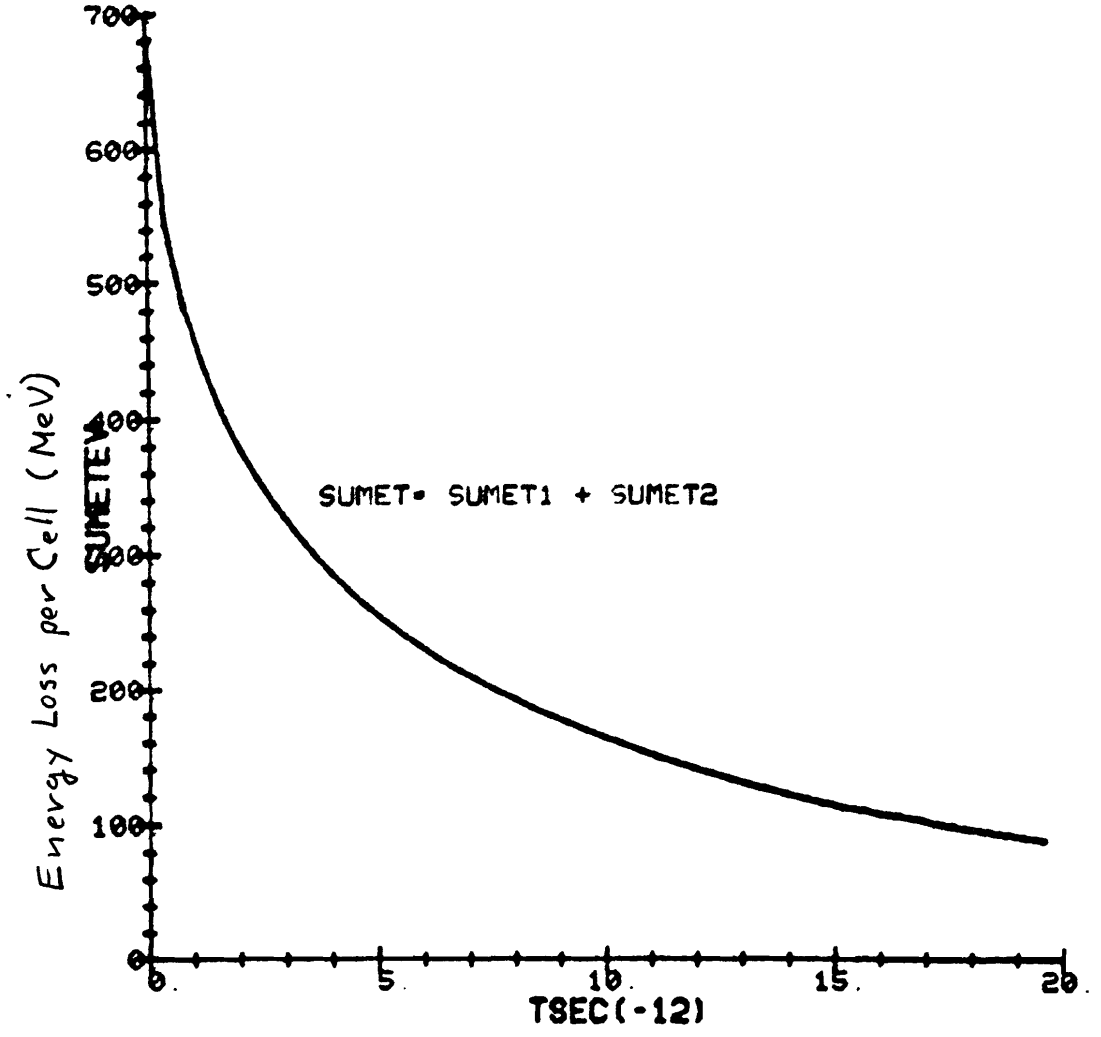

Fig. 10 -- Wake potential for the SLAC linac structure for a point bunch of 5 x 10^8 electrons.

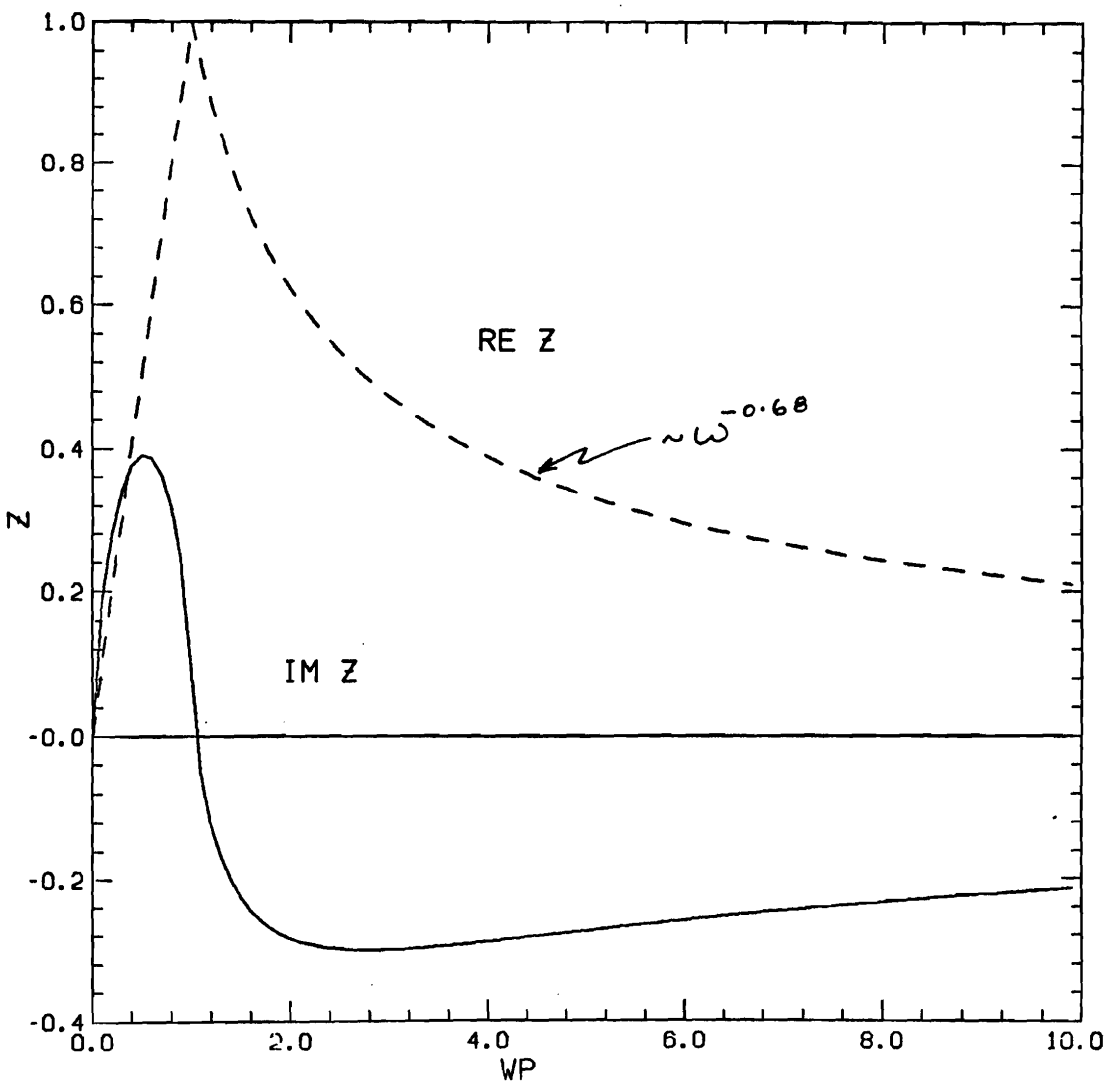

Fig. 11 -- SPEAR impedances normalized to a frequency of 2π x 1.2 GHz and a peak value of 8000 ohms for Re Z.